An Optimal ZVS Angle Selection for Constant Current Charging of EV's Battery in Series-Series Compensated Wireless Power Transmission System

Yongbin Jiang, Junwen Liu, Xiufang Hu, Laili Wang, Yue Wang, Gaidi Ning
School of the Electric Engineering, Xi'an Jiaotong University
Xi'an 710049 China
jiangyongbin@stu.xjtu.edu.cn

***Abstract*—In this paper, first, to realize the constant current charging for EV's Battery and ZVS operation of primary inverter simultaneously, variable frequency and phase shift control strategy (VF-PSC) is adopted and the optimal operation frequency range (OOFR) is obtained. Second, a three loop control strategy (TLCS) is proposed to make the system work accurately at any points of this OOFR by adjusting the zero voltage switching angle (ZVSA). Third, to achieve the maximum efficiency of the system, a maximum efficiency point tracking strategy (MEPT) is proposed to maximize the system efficiency by changing the ZVSA continuously in OOFR. The combination between TLCS and MEPT is prominent and excellent because it realizes constant current charging, ZVS operation, and maximum system efficiency simultaneously, which dramatically reduces EMI, improves the security and reliability, and saves electrical energy. Finally, a 500W WPT system (WPTS) is built to verify the correctness of theoretical analysis and the effectiveness of the proposed control strategy.**

***Index Terms*—Variable frequency and phase shift control strategy (VF-PSC), the optimal operation frequency range (OOFR), zero voltage switching angle (ZVSA), wireless power transmission (WPT), maximum efficiency point tracking strategy (MEPT)**

I. Introduction

Power transfer plays an important role in human life and many researchers are devoting themselves to making it safer, more convenient and more efficient. Meanwhile, electrical vehicle (EV) had achieved rapid development in the past decades. But the traditional plug-in charging methods for EV's battery may cause many problems. Therefore, WPT technology was applied in this application for its safety, convenience and other merits [1]–[5].

To realize ZVS operation of primary inverter and constant current charging for EV's battery, there are two main methods. One uses some DC/DC converters to regulate the output current and uses the fixed operation frequency to realize ZVS operation [6]–[8]. However, this method relatively has poor efficiency with a high cost. The other [4], [9], [10] uses variable frequency and phase shift control strategy (VF-PSC) to realize these two control aims. However, this method cannot make full use of the system characteristics due to the constant ZVSA and cannot achieve the maximum efficiency of the whole system.

In this paper, first, the variable frequency and phase shift control strategy (VF-PSC) is adopted. Meanwhile, the operation frequency range to make the system realize constant output current and ZVS operation of inverter simultaneously is obtained and defined as optimal operation frequency range (OOFR). Furthermore, a three loop control strategy (TLCS) is proposed to make the system work in any points of this OOFR by adjusting the zero voltage switching angle (ZVSA). Moreover, to achieve the maximum system efficiency, a maximum efficiency point tracking strategy (MEPT) is proposed to maximize the system efficiency by changing the ZVSA continuously when constant output current is realized. A 500W WPT system (WPTS) is built to verify the correctness of theoretical analysis and the effectiveness of the proposed control strategy.

II. Basic Analysis of the WPTS

A. The trans-conductance gain and input impedance angle

The topology of a typical SS-type WPT system is shown in Fig. 1, which is composed of a high frequency inverter, a resonant network and a rectifier. The corresponding equivalent AC circuit is shown in Fig. 2. In the analysis of an SS-type WPT system, fundamental harmonic approximation is normally used since the fundamental component of the current in resonant tank is much larger than harmonics. The load resistor R_{L} is replaced by its equivalent AC resistance R_{E}, which equals to $8R_{\mathrm{L}}/\pi^2$. To simplify the calculation, the resonant frequency ω_0 for both sides are equal. The switching frequency is ω_{s}. Consequently, the per-unit of ω_{s} is defined as $\omega_{\mathrm{n}} = \omega_{\mathrm{s}}/\omega_0$.

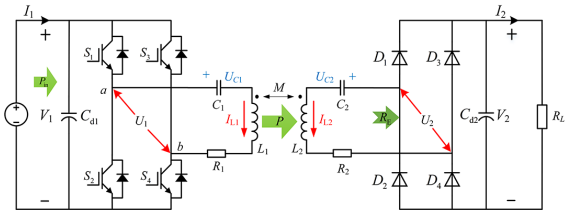

Fig. 1. Schematic of the WPTS

To control the charging current I_2 and ZVS operation of inverter, the VF-PSC is applied in Fig. 1. The operation waveforms of primary inverter are shown in Fig. 3. U_1 is the

fundamental waveform of the output voltage of inverter v_{ab} with phase shift angle $D\pi$, and I_{L1} is primary inductor current. Consequently, the phase between U_1 and I_{L1} is the input impedance angle (IIA) of resonant network, φ_{IIA}. Meanwhile, the angle for ZVS operation is defined as φ_{ZA}. The trans-conductance gain of system (TCGS) is defined as G_{ivsys}, that can be obtained by (1).

With the parameters listed in Table I, when k=0.2, the TCGS as a function of duty cycle D and operation frequency ω_{n} is calculated and plotted in Fig. 4(a). Based on Fig. 2, the input impedance angle (IIA), φ_{IIA}, with R_1 and R_2 neglected, can be calculated in equation (2).

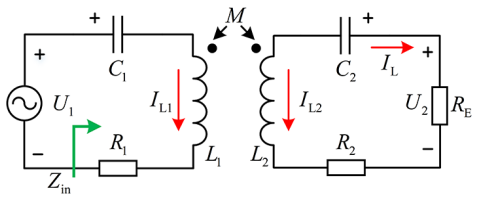

Fig. 2. Equivalent circuit

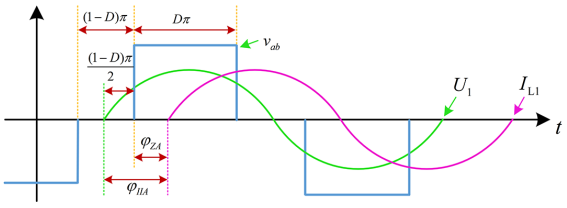

Fig. 3. Operation waveforms of primary inverter

Similarly, With the parameters listed in Table I and different coupling coefficient, the φ_{IIA} as a function of operation frequency ω_{n} and load resistor R_{L}, is calculated and plotted in Fig. 4(b).

TABLE I
PARAMETERS USED IN CALCULATION

Symbol	Quantity	Value
$L_1,\ L_2$	resonant inductances	116.864μH
$C_1,\ C_2$	resonant capacitances	30nF
ω_0	resonant angular frequency	5.34×10^5rad/s
f_0	resonant frequency	85kHz

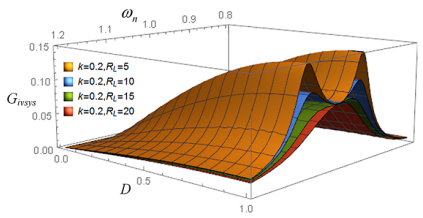

(a)

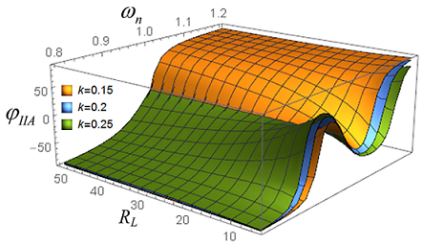

(b)

Fig. 4. Characteristics of WPTS: (a) G_{ivsys} versus D and ω_{n}, when k=0.2 (b) φ_{IIA} versus R_{L} and ω_{n}, with different k.

B. Zero Voltage Switching Angle (ZVSA)

As shown in Fig. 3, the IIA can be obtained as

$$\varphi_{\mathrm{IIA}} = \varphi_{\mathrm{ZA}} + \frac{(1-D)\pi}{2} \tag{3}$$

To reduce switching losses and EMI, and enhance the system efficiency and reliability, ZVS should be achieved in primary inverter, which means $\varphi_{\mathrm{ZA}} \geq 0$ at least. Usually, $1 > D > 0$, then $\varphi_{\mathrm{IIA}} > \varphi_{\mathrm{ZA}}$.

C. The Optimal Operation Frequency Range (OOFR)

When input dc voltage V_1 and output current I_2 are constant, the TCGS is constant. According to (1), if assigning the TCGS equals K_x, then the corresponding duty cycle can be solved by (4). According to (3), the critical conditions for ZVS operation when $\varphi_{\mathrm{ZA}} = 0$ can be obtained, that is

$$\varphi_{\mathrm{IIAmin}} = \frac{(1-D)\,\pi}{2} \tag{5}$$

Then, according to (5), define D_{min} as $(1-D)/2$. With the parameters listed in Table I, when K_x = 0.01, 0.02, 0.04 respectively, the corresponding D_{min} which maintains constant

$$G_{\mathrm{ivsys}} = \frac{8kL_2\omega_{\mathrm{n}}^3 \sin\left[D\pi/2\right]}{\sqrt{L_1L_2\left(64R_{\mathrm{L}}^2\omega_{\mathrm{n}}^2(-1+\omega_n^2)^2 + \pi^4L_2^2\omega_0^2(-1+2\omega_{\mathrm{n}}^2+(-1+k^2)\,\omega_{\mathrm{n}}^4)^2\right)}} \tag{1}$$

$$\varphi_{\mathrm{IIA}} = \arctan\left[\frac{\mathrm{Im}\left[Z_{\mathrm{in}}\right]}{\mathrm{Re}\left[Z_{\mathrm{in}}\right]}\right] = -\frac{180}{\pi}\arctan[\frac{\left(-1+\omega_{\mathrm{n}}^2\right)\left(-64R_{\mathrm{L}}^2\omega_{\mathrm{n}}^2+\pi^4L_2^2\omega_0^2\left(-1+2\omega_{\mathrm{n}}^2+\left(-1+k^2\right)\omega_{\mathrm{n}}^4\right)\right)}{8\pi^2k^2L_2R_{\mathrm{L}}\omega_0\omega_{\mathrm{n}}^5}] \tag{2}$$

$$D = \frac{2}{\pi}\arcsin\left[\frac{K_x}{8kL_2\omega_{\mathrm{n}}^3}\sqrt{L_1L_2\left(64R_{\mathrm{L}}^2\omega_{\mathrm{n}}^2(-1+\omega_{\mathrm{n}}^2)^2+\pi^4\omega_0^2L_2^2(-1+2\omega_{\mathrm{n}}^2+(-1+k^2)\,\omega_{\mathrm{n}}^4)^2\right)}\right] \tag{4}$$

output current, are plotted in Fig. 5(a). When K_x decreases, $D_{\min}$ increases which corresponds to the control variable D decreasing, and the operation frequency range of $\omega_{\rm n}$ magnifies. However, there are only parts of combinations of $\omega_{\rm n}$ and D which can realize ZVS operation.

To find the OOFR, the per-unit value of $\varphi_{\rm IIA}$ is defined as $\varphi_{\rm IIApu} = \varphi_{\rm IIA}/180$. Simultaneously, with the same parameters in Table I, $\varphi_{\rm IIApu}$ versus $\omega_{\rm n}$ is plotted in Fig. 5(a). When $\omega_{\rm n} > 1$, the purple intersections of $D_{\min}$ and $\varphi_{\rm IIApu}$, A_1, A_2, A_3 are the lower limit frequencies with different K_x. When D=1 and controlling the TCGS equals different K_x, the corresponding upper limit frequencies are the green points, B_1, B_2, B_3 respectively, which are equivalent to the frequencies when $D_{\min}$=0. Then, the OOFRs in different K_x are from A_x to B_x (x =1,2,3).

The corresponding ZVSA curves versus $\omega_{\rm n}$ with K_x=0.01, 0.02, 0.04, are plotted in Fig. 5(b). As the K_x decreases, the OOFR increases gradually and the maximum value of ZVSA increases accordingly.

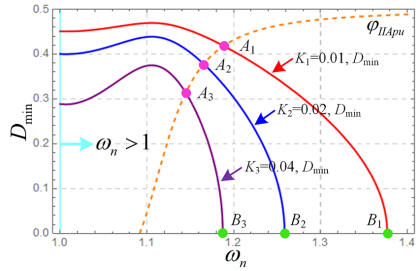

(a)

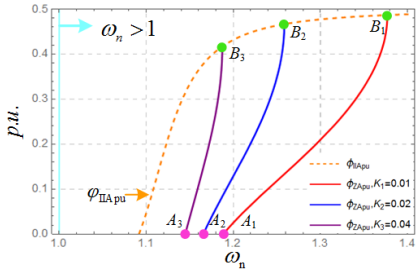

(b)

Fig. 5. The OOFRs with k=0.2 and $R_{\rm L}$=10Ω, (a) the critical condition for ZVS and constant current charging with K_x=0.01, 0.02, 0.04 respectively, (b) the corresponding ZVSA versus $\omega_{\rm n}$ with K_x=0.01, 0.02, 0.04 respectively.

D. The Optimal Operation Frequency Point

Based on the previous analysis in this paper, the whole system realizes the constant current charging and ZVS operation of primary inverter simultaneously in the OOFR. However, there is only one frequency in the OOFR to achieve maximum system efficiency, which is defined as the optimal operation frequency point (OOFP).

First, the whole system efficiency should be analyzed. The power losses of the WPTS include the losses of inverter, the losses of the resonant network and the losses of the rectifier. When the primary inverter realizes ZVS operation, the losses of inverter mainly contains conduction loss, which can be assumed as constant and included in ESRs R_1. Similarly, the secondary rectifier conduction loss can be included in ESRs R_2 for simplicity. Based on Fig.2, the system efficiency except the switching losses of inverter can be represented by (6).

Then, based on $\partial\eta_{\rm sys}/\partial R_{\rm L} = 0$, the optimal operation frequency point $\omega_{\rm nopt}$ (OOFP) can be obtained by

$$\omega_{\rm nopt} = \frac{\pi^2 L_2}{\sqrt{-0.5(\pi^2 R_2 + 8R_{\rm L})^2 + \pi^4\omega_0^2 L_2^2}} \tag{7}$$

With the parameters in Table I and assuming $R_1 = 1\Omega$ and $R_2 = 1\Omega$, the system efficiency as a function of k and $R_{\rm L}$ is calculated and plotted in Fig. 6(a). When $R_{\rm L}$ is fixed, the whole system efficiency except the switching losses of inverter is a single peak function of $\omega_{\rm n}$. These corresponding OOFPs are marked as E_x (x=1 4) with different $R_{\rm L}$. As the $R_{\rm L}$ gradually increases, the OOFP gradually increases. To achieve the maximum system efficiency, the OOFPs of inverter should be selected in consideration of the OOFRs with different $R_{\rm L}$.

When $R_{\rm L}$ is fixed, based on (7), the corresponding OOFP is fixed. However, the OOFRs are varied in different operation situations. For example, as shown in Fig. 6(b), when the TCGS changes, the OOFR changes accordingly. In summary, there are three situations where the whole system achieves the maximum efficiency, which are listed in Table II. The location of OOFP may appear at the left-side, the right-side or the interior of the OOFR. The theoretical selected frequency points are listed in Table II.

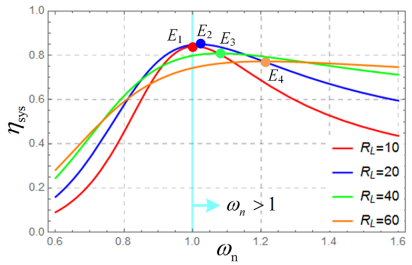

(a)

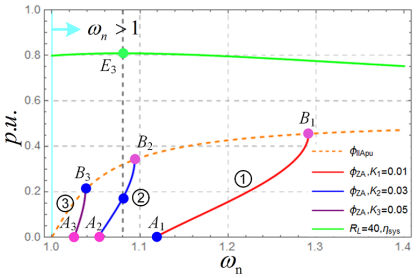

(b)

Fig. 6. (a) The system efficiency versus $\omega_{\rm n}$ with k=0.2 and different $R_{\rm L}$, (b) the relationship between OOFPs and OOFRs with different K_x when k=0.2 and $R_{\rm L} = 40\Omega$.

$$\eta_{sys}=\frac{8\pi^2k^2L_1L_2R_{\mathrm{L}}\omega_0^2\omega_{\mathrm{n}}^4}{R_1(\pi^2R_2+8R_{\mathrm{L}})^2\omega_{\mathrm{n}}^2+k^2L_1L_2\pi^2\left(\pi^2R_2+8R_{\mathrm{L}}\right)\omega_0^2\omega_{\mathrm{n}}^4+\pi^4R_1\omega_0^2L_2^2(\omega_{\mathrm{n}}^2-1)^2} \tag{6}$$

TABLE II
THE SELECTED OPERATION FREQUENCY POINT

Situation	OOFR	Location	Selected frequency point
①	$[\omega_{\mathrm{A1}},\omega_{\mathrm{B1}}]$	Left	ω_{A1}
②	$[\omega_{\mathrm{A2}},\omega_{\mathrm{B2}}]$	Middle	ω_{E3}
③	$[\omega_{\mathrm{A3}},\omega_{\mathrm{B3}}]$	Right	ω_{B3}

III. THE MEPT CONTROL STRATEGY

A. Description of TLCS

The control block diagram of TLCS is shown in Fig. 7. The control strategy includes three closed loops: the inner loop of the RMS value of primary resonant current, the outer loop of the CC output and the ZVSA loop of primary inverter. The operation principal of these loops is briefly explained as follows.

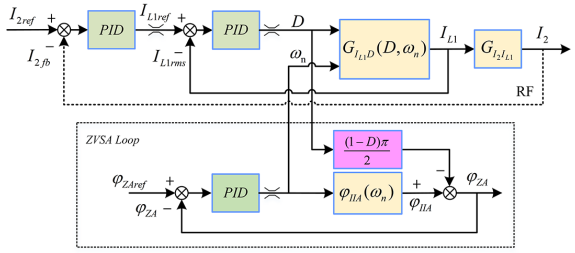

Fig. 7. The control block diagram of TLCS

I_{L1ref} is the RMS value instruction of the inner current loop of primary resonant current I_{L1} and the corresponding feedback signal I_{L1rms}, is detected by analog circuit. The aim of the inner current loop is to improve the system dynamic response of the WPTS and to restrict the amplitude of primary resonant current to a safe operating region.

Usually, the processer of primary inverter receives the instructions $I_{2\mathrm{ref}}$ from EV's BMS in practical application, and controls the charging current I_2 to track $I_{2\mathrm{ref}}$. The processor of secondary rectifier samples I_2 and sends it to the primary processor through radio frequency (RF) communication. Based on $I_{2\mathrm{ref}}$ and $I_{2\mathrm{fb}}$, the primary processor calculates the instructions of inner current loop through PID algorithm.

To realize ZVS operation of primary inverter absolutely, φ_{ZA} must be larger than zero. However, D changes for controlling CC output in real time, which leads to φ_{ZA} changing continually. Therefore, the phase loop and current loop are highly coupled. Fortunately, according to (3), a simple decoupling control for ZVSA loop is proposed which is marked in bright purple. Simultaneously, to decrease the effect of ZVSA loop to inner current loop, the setting time of ZVSA loop is relatively larger than that of inner current loop. φ_{ZAref} is a variable reference angle for realizing ZVS and the corresponding feedback signal is φ_{ZA} which is detected by external circuit [11]. Based on φ_{ZAref} and φ_{ZA}, the primary processor calculates the operation frequency of inverter through PID algorithm.

B. The Principle of MEPT

There is an important assumption in the analysis of the maximum efficiency point: the WPT system only has the ESR losses. In Section II, the power losses in the inverter and the rectifier have been converted into the ESR losses. The MEPT control scheme fixes the charging current I_2 and adjusts the operation frequency of inverter continually by setting different φ_{ZAref} in TLCS.

In the system shown in Fig. 7, the control variable D is used to regulate the output current I_2 and the control variable ω_{n} is used to regulate the φ_{ZA}. Based on TLCS, by changing the φ_{ZAref}, the whole system will operate in different steady-state operation points. The controller records the efficiency for each step of the perturbation and regulation. The direction of φ_{ZAref} perturbation is maintained constant for the next step if the efficiency gets higher; otherwise, it will reversed. Fig. 8 shows this flowchart.

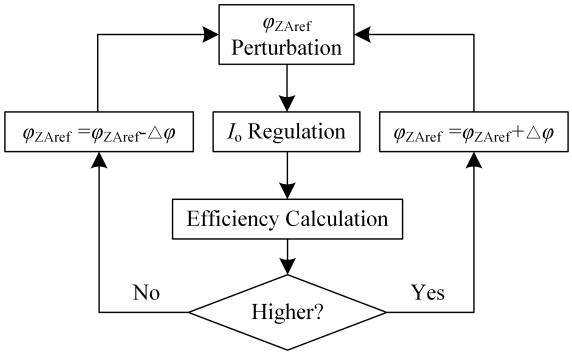

Fig. 8. Flowchart of the MEPT control scheme

IV. EXPERIMENT VERIFICATION

A. Experimental Prototype

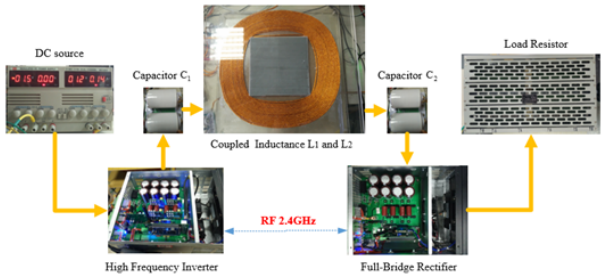

Fig. 9. Experimental prototype

TABLE III
RESONANT NETWORK PARAMETERS

Symbol	Value	Symbol	Value
L_1	118.34μH	L_2	118.56μH
C_1	29.92nF	C_2	29.88nF
R_1	0.12Ω	R_2	0.11Ω
f_1	84.56kHz	f_2	84.58kHz
k	0.16-0.22	$R_{\rm L}$	10Ω
V_1	60V	ω_0	5.31×10^5rad/s

To verify the performance of the proposed TLCS, a 500W experimental prototype shown in Fig. 9 is built up. The prototype includes a dc source, a high frequency inverter, a SS resonant network, a full-bridge rectifier and a sliding rheostat. The voltage and current values of the sliding rheostat are sent to primary control system by 2.4GHz RF module. The experiment parameters of the resonant network are given in Table III.

B. Steady state waveforms in ZVSA loop

Based on the proposed TLCS, the steady state experimental results are carried out as follows. When V_1= 60V, $R_{\rm L}$= 10Ω, $I_{2\rm ref}$= 3.6A, setting $\varphi_{\rm ZAref}$ = 0° and $\varphi_{\rm ZAref}$ = $\varphi_{\rm ZAmax}$ respectively, then the corresponding experimental steady state waveforms are shown in Fig. 10. Therefore, the lower and upper frequencies can be measured by setting 0° and $\varphi_{\rm ZAmax}$ when maintaining constant K_x.

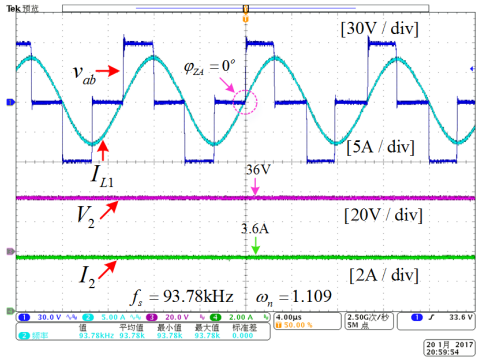

(a)

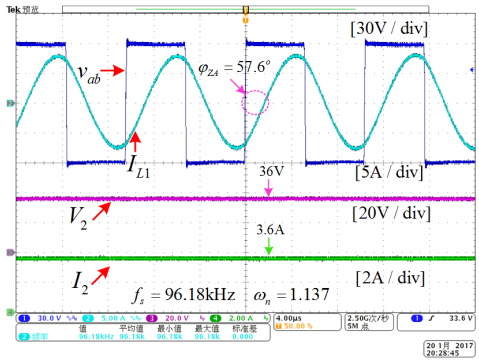

(b)

Fig. 10. Steady state waveforms of ZVS operation, when V_1= 60V, $R_{\rm L}$= 10Ω, $I_{2\rm ref}$= 3.6A, (a) $\varphi_{\rm ZAref}$ = 0°, (b) $\varphi_{\rm ZAmax}$ = 57.6°.

C. The Whole System Efficiency

To verify the relationship between the OOFR and OOFP, based on the TLCS, the whole experimental system efficiency curves and the theoretical calculated OOFPs are plotted in Fig.11, by setting K_x = 0.01, 0.03 and 0.04 respectively, with k=0.22 and $R_{\rm L}$ = 40Ω.

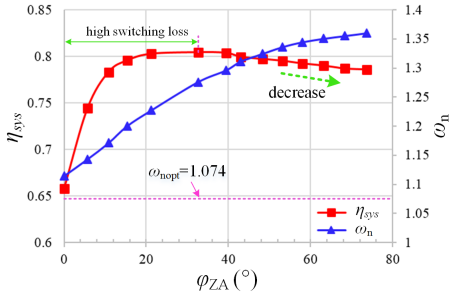

(a)

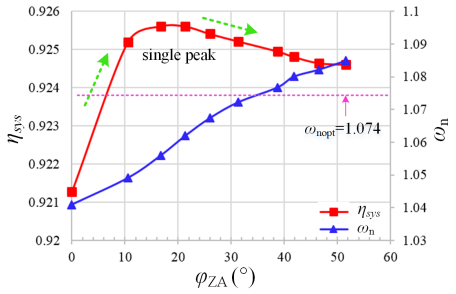

(b)

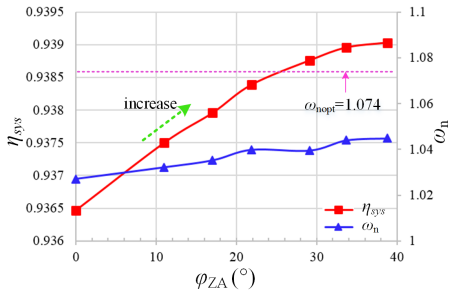

(c)

Fig. 11. The System efficiency and the experimental operation frequencies $\omega_{\rm n}$, when V_1= 60V, $R_{\rm L}$= 40Ω and k= 0.22, (a) K_x=0.01, (b) K_x=0.03,(c) K_x=0.04.

The blue line is the system efficiency, the red line is the corresponding frequency of $\varphi_{\rm ZA}$ and the purple dotted line is the OOFP. In Fig. 11(a), when K_x is relativity small and the OOFP is smaller than $\omega_{\rm n}$, which means that the OOFP is located in the left of OOFR, in which case, from the previous analysis the system efficiency is monotonically decreasing versus $\varphi_{\rm ZA}$. However, the experimental system efficiency curve is a single peak function of $\varphi_{\rm ZA}$ because the high switching loss of inverter exists when $\varphi_{\rm ZA}$ stays near zero. In Fig. 11(b), the OOFP is crossed with $\omega_{\rm n}$, which means that the OOFP is located within of OOFR, in which case,

a peak system efficiency is exist. In Fig. 11(c), the OOFP is greater than ω_{n}, which means that the OOFP is located in the right of OOFR, in which case, the system efficiency is monotonically increasing versus φ_{ZA}. Compared with the efficiency curves in Fig. 11, except Fig. 11(a) the experiment result is in a good match with the theoretical analysis.

V. Conclusion

In this paper, VF-PSC is adopted to realize CC charging for EVs and ZVS operation. Then, the optimal operation frequency range using VF-PSC in a specific condition, is carried out in detail. The TLCS is proposed to make the system work in any points of this OOFR by adjusting the ZVSA. Moreover, to achieve the maximum efficiency of the system, a MEPT is proposed to maximize the system efficiency by changing the ZVSA continuously when realizing constant charging current. The combination between TLCS and MEPT makes the system realize constant current charging, ZVS operation, and the maximum system efficiency simultaneously, which dramatically reduces EMI, improves security and reliability, and saves electrical energy. The experimental results give a good agreement with the theoretical analysis.

References

[1] F. Musavi and W. Eberle, "Overview of wireless power transfer technologies for electric vehicle battery charging," *Iet Power Electronics*, vol. 7, no. 1, pp. 60–66, 2014.

[2] D. Ongayo and M. Hanif, "An overview of single-sided and double-sided winding inductive coupling transformers for wireless electric vehicle charging," in *Future Energy Electronics Conference*, 2015, pp. 1–6.

[3] G. Buja, M. Bertoluzzo, and K. N. Mude, "Design and experimentation of wpt charger for electric city car," *IEEE Transactions on Industrial Electronics*, vol. 62, no. 12, pp. 7436–7447, 2015.

[4] Q. Chen, S. C. Wong, C. K. Tse, and X. Ruan, "Analysis, design, and control of a transcutaneous power regulator for artificial hearts." *IEEE Transactions on Biomedical Circuits & Systems*, vol. 3, no. 1, p. 23, 2009.

[5] Y. Jiang, Y. Wang, J. Liu, X. Hu, S. Yin, Z. Wang, and L. Wang, "An optimal parameters design methodology of series-series resonant tank of wireless power transmission system for battery charging," in *2017 IEEE Applied Power Electronics Conference and Exposition (APEC)*, March 2017, pp. 1600–1605.

[6] H. Li, J. Li, K. Wang, W. Chen, and X. Yang, "A maximum efficiency point tracking control scheme for wireless power transfer systems using magnetic resonant coupling," *IEEE Transactions on Power Electronics*, vol. 30, no. 7, pp. 3998–4008, July 2015.

[7] D. Ahn and S. Hong, "Wireless power transfer resonance coupling amplification by load-modulation switching controller," *IEEE Transactions on Industrial Electronics*, vol. 62, no. 2, pp. 898–909, Feb 2015.

[8] T. D. Yeo, D. Kwon, S. T. Khang, and J. W. Yu, "Design of maximum efficiency tracking control scheme for closed-loop wireless power charging system employing series resonant tank," *IEEE Transactions on Power Electronics*, vol. 32, no. 1, pp. 471–478, Jan 2017.

[9] Q. Chen, L. Jiang, J. Hou, X. Ren, and X. Ruan, "Research on bidirectional contactless resonant converter for energy charging between evs," in *IECON 2013 - 39th Annual Conference of the IEEE Industrial Electronics Society*, Nov 2013, pp. 1236–1241.

[10] P. Tan, H. He, and X. Gao, "Phase compensation, zvs operation of wireless power transfer system based on sogi-pll," in *2016 IEEE Applied Power Electronics Conference and Exposition (APEC)*, March 2016, pp. 3185–3188.

[11] Y. Jiang, Y. Wang, J. Liu, X. Li, and L. Wang, "An accurate phase detection method for realizing zvs of high frequency inverter in wireless power transmission," in *2017 IEEE 3rd International Future Energy Electronics Conference and ECCE Asia (IFEEC 2017 - ECCE Asia)*, June 2017, pp. 1380–1384.